

Spiking Neural Networks for Radio Frequency Interference Detection in Radio Astronomy

Nicholas J. Pritchard^{1, 2*}, Andreas Wicencec^{1†},
Mohammed Bennamoun^{2†}, Richard Dodson^{1†}

¹International Centre for Radio Astronomy Research, University of Western Australia, 7 Fairway, Crawley, 6009, WA, Australia.

²School of Physics, Mathematics and Computing, University of Western Australia, 35 Stirling Highway, Crawley, 6009, WA, Australia.

*Corresponding author(s). E-mail(s):

nicholas.pritchard@research.uwa.edu.au;

Contributing authors: andreas.wicencec@icrar.org;

mohammed.bennamoun@uwa.edu.au; richard.dodson@icrar.org;

[†]These authors contributed equally to this work.

Abstract

Spiking Neural Networks (SNNs) promise efficient spatio-temporal data processing owing to their dynamic nature. This paper addresses a significant challenge in radio astronomy, Radio Frequency Interference (RFI) detection, by reformulating it as a time-series segmentation task inherently suited for SNN execution. Automated RFI detection systems capable of real-time operation with minimal energy consumption are increasingly important in modern radio telescopes. We explore several spectrogram-to-spike encoding methods and network parameters, applying first-order leaky integrate-and-fire SNNs to tackle RFI detection. To enhance the contrast between RFI and background information, we introduce a divisive normalisation-inspired pre-processing step, which improves detection performance across multiple encoding strategies. Our approach achieves competitive performance on a synthetic dataset and compelling results on real data from the Low-Frequency Array (LOFAR) instrument. To our knowledge, this work is the first to train SNNs on real radio astronomy data successfully. These findings highlight the potential of SNNs for performing complex time-series tasks, paving the way for efficient, real-time processing in radio astronomy and other data-intensive fields.

Keywords: Spiking neural networks, radio astronomy, RFI detection, time-series segmentation

Spiking Neural Networks (SNNs) are inspired by how biological neurons communicate. Instead of using continuous signals, as in Artificial Neural Networks (ANNs), they transmit information in discrete spikes or pulses, closer to how natural neurons fire [1]. ANNs have proven to be highly effective, especially when deployed on conventional computing hardware platforms, and they excel in numerous tasks when combined with large datasets. The central question remains whether SNNs can reliably achieve comparable or superior results by mimicking biological neurons more closely while using less energy and computational power, particularly when running on neuromorphic computing systems [2]. The potential for SNNs to outperform traditional models hinges on developing efficient neuromorphic hardware and identifying data-intensive applications that can exploit the temporal dynamics unique to SNNs [3]. While SNNs have shown promise in several domains, particularly those leveraging neuromorphic sensing hardware, tackling increasingly demanding tasks is vital to moving the field forward.

Radio astronomy involves coordinating increasingly complex observatories and massive computing facilities to process the increasingly vast amount of data generated by observing the cosmos [4]. One of the primary challenges in this field is dealing with Radio Frequency Interference (RFI), which refers to unwanted radio signals originating from human-made or terrestrial sources. RFI can significantly contaminate radio astronomy data, and detecting these polluted regions in observed spectrograms and subsequently removing them from further analysis is crucial for preserving the scientific integrity of the observations. The need for adaptive, data-driven RFI detection methods grows as radio telescopes become more sensitive and RFI becomes more pervasive. While many factors contribute to increased RFI prevalence, the sudden increase in low-Earth orbit satellites operating over more of the radio spectrum is chief among them, even in sparsely populated parts of the Earth where terrestrial sources are less prevalent [5–7]. Traditional approaches to RFI detection often rely on cumulative-sum algorithms fine-tuned to specific instruments and environments [8], in combination with solutions built into the interferometry hardware [9, 10]. Contemporary experimental machine learning techniques based on UNet-like CNNs [11–13], anomaly detection schemes [14, 15] or vision-transformer models [16] offer competitive, and sometimes superior, results, albeit with high operational costs and a need for extensive training data [17].

Both conventional and machine-learned approaches treat RFI detection as a two-dimensional semantic segmentation or anomaly detection problem, where spectrograms, or ‘visibilities,’ are treated like images. Although effective, existing two-dimensional approaches to RFI detection necessitate completing an entire observation before processing can commence. This is a significant limitation as data destined to be removed is stored and processed in costly high-performance computing facilities [4]. As such, there is a strong imperative in the field to develop RFI detection techniques

that are accurate and capable of operating in near real-time, with minimal energy consumption, and where applicable, minimal training data [14, 17].

The time-varying nature of radio astronomy data and its spectrographic characteristics suggest that this domain could benefit from SNNs and neuromorphic computing [18]. Despite this potential, only a few attempts have been made to apply SNNs within radio astronomy [19]. More specifically, regarding RFI detection, only one existing study employs SNNs [20]. This work utilised ANN-to-SNN conversion in an auto-encoder-based anomaly detection framework. While it demonstrated operational benefits, the approach did not fully take advantage of the inherent time-varying aspects of radio astronomy observations, leaving much of the potential for SNNs untapped in this area.

Previous applications of SNNs to spectrographic data, such as audio processing, have primarily focused on classification tasks [21, 22]. In such tasks, a time-varying input is processed, but the final output is reduced to a single value or decision derived from the final layer of the network. However, the problem of RFI detection requires the output to retain the same temporal and spatial resolution as the input data. In this work, we reformulate RFI detection as a time-series segmentation problem, where the network must output a prediction that spans the same time and frequency dimensions as the input spectrogram to explore how well first-order leaky-integrate and fire (LiF) spiking neurons can capture temporal information in this task. To our knowledge, this is the first time SNNs have been applied to this kind of task, and until now, it has been unknown whether backpropagation through time (BPTT) can handle the complexity of such tasks.

Transitioning from synthetic datasets to real radio astronomy data introduces a significant increase in noise and variability. To assist in handling this challenge, we introduce a pre-processing technique inspired by divisive normalisation, a sensory adaptation mechanism rooted in neuroscience [23]. Divisive normalisation has been studied extensively and incorporated into image segmentation networks [24], and we have adapted the basic concepts into a spectrogram pre-processing step. This pre-processing technique relies only on values from a single preceding time step, effectively increases the contrast between RFI and background signals and, critically, applies universally to all downstream spike-encodings. This technique increases spike sparsity in all encodings and significantly improves performance on the synthetic and real radio astronomy datasets we investigate in this work.

This paper provides a robust formulation of RFI as a time-series segmentation task appropriate for direct SNN execution, investigates encoding visibility data with latency, rate, delta-modulation, delta-exposure and three distinct variations on step-forward encoding, extensive hyper-parameter optimisation, a divisive normalisation inspired pre-processing step which greatly improves detection performance across several encoding methods, and results for SNNs trained and optimised with each encoding for a synthetic dataset simulating the Hydrogen Epoch of Reionisation Array (HERA) in South Africa, and a real RFI detection dataset derived from the Low-Frequency Array (LOFAR) instrument in the Netherlands with comparison to identically sized ANN feed-forward networks. This paper builds upon our previously presented work [25], extending it in several important ways. The delta-exposure encoding method and

divisive-normalisation-inspired pre-processing step are previously unseen techniques. We provide more comprehensive hyper-parameter optimisation extending into network depth and width in addition to a more extensive analysis of the resulting parameter space. Lastly, by including results for the real LOFAR dataset, we present the first study demonstrating the application of from-scratch trained SNNs on real radio astronomy data. In doing so, we achieve state-of-the-art RFI detection performance on the synthetic HERA dataset and competitive results on the real LOFAR dataset, demonstrating the efficacy of our approach while employing small multi-layer feed-forward SNNs. This investigation demonstrates the capability of SNNs to perform a data-intensive complex time-series segmentation task in the form of RFI detection with relatively simple network architectures, paving the way for more sophisticated SNN-based RFI detection schemes and critically finding a scientifically impactful problem in which SNNs and neuromorphic computing may hold unique advantages over contemporary methods.

Results

RFI Detection as Time-Series Segmentation

The signal chain in a radio interferometer array observatory, generally speaking, first involves correlating raw voltage signals from antennae, transforming the data into complex-valued ‘visibilities’ $V(v, T, b)$, which vary in frequency, time and baseline (pair of antennae) [26]. At this stage in the processing chain, RFI detection involves producing a boolean mask of ‘flags’ $G(v, T, b)$ that vary in the same parameters but are binary-valued. These binary masks are used in subsequent signal processing steps to speed up the collation of visibilities into image cubes which are then eventually handed off to astronomers to begin scientific processing. Increasing the throughput of RFI detection directly improves the throughput of data to end-user scientists.

Previous supervised approaches to RFI detection via machine learning formulate the problem as

$$\mathcal{L}_{sup} = \min_{\theta_n} \mathcal{H}(m_{\theta_n}(V(v, T, b)), G(v, T, b)), \quad (1)$$

where θ_n are the parameters of some classifier m and \mathcal{H} is an entropy-based similarity measure [14]. We exploit the time-varying nature of this information and, therefore, include additional spike encoding and decoding steps and push the similarity measure inwards, operating on each element of the resulting time-series.

$$\mathcal{L}_{sup} = \min_{\theta_n} (\sum_t^T \mathcal{H}(m_{\theta_n}(E(V(v, t, b))), F(G(v, t, b)))) \quad (2)$$

where E is an input encoding function and F is an output encoding function. Both functions introduce a new integer exposure parameter, controlling the spike train length for each time step in the original spectrogram.

This formulation tasks a classifier to segment the time series, in this case, as boolean values rather than a two-dimensional image. In the case of an ANN, the encoding and decoding functions are the identity. This formulation leaves encoding and decoding visibility data as spikes for this specific task open for experimentation. The spike encoding process involves stretching the original time steps in the spectrograms into

longer exposures, allowing the SNN to react to the current input. We experimented with seven encoding methods, which we briefly outline. The methods section presents detailed formulations and examples of each encoding approach.

Latency

Latency encoding transforms pixel intensity into spike timings. This method benefits from a deterministic decoding method and a fixed number of spikes.

Rate

Rate encoding translates pixel intensities into spike rates, interpreting intensity as the probability of a Poisson process for each exposure time. Rate decoding is inherently more stochastic than most other methods, so achieving reliable results in this task is difficult. Moreover, spike counts increase proportionally to the exposure time.

Delta-Modulation

Delta-modulation encoding fires a positive polarity spike when a positive difference between two time steps passes a threshold and a negative polarity spike when a negative difference passes a threshold. Delta-modulation is easily decoded but can struggle with frequency-localised RFI.

Delta-Exposure

Delta-exposure encoding is similar to delta-modulation but includes time for the network to react to each time step in the original spectrogram.

Step-Forward

Step-forward encoding comes from Speech2Spikes [21] and is inspired by encoding vocal spectrograms. This method encodes the input’s transient and cumulative properties in two separate sections, doubling the input-width. We experimented with three sub-variants of this method, presenting spikes only at the first exposure time (first exposure), at a time proportional to the original input intensity (latency exposed) and at all exposure time steps (direct exposure).

Figure 1 outlines our complete approach to supervised RFI detection with SNNs using delta-exposure encoding as an example. Notably, the input width of the SNN either exactly matches or doubles (in the case of step-forward encodings) the number of input frequency channels (32 in this case). For training purposes, we slice each spectrogram into 32×32 pixel patches and encode each into a spike train using the swappable encoding method. The entire spike train is fed into the SNN along the time axis, and supervision is performed on the SNN’s output spike train. At inference and final testing, the SNN’s output spike train is then decoded into another patch that is then re-stitched into a complete spectrogram for accuracy testing. This task is challenging for an SNN as we present each original time step in the spectrogram precisely once; identifying features that span the entire spike train requires the network to retain some of this information in the leaky dynamics of the neurons themselves; these results represent a baseline level of performance given what is as lightweight a network as possible for this task.

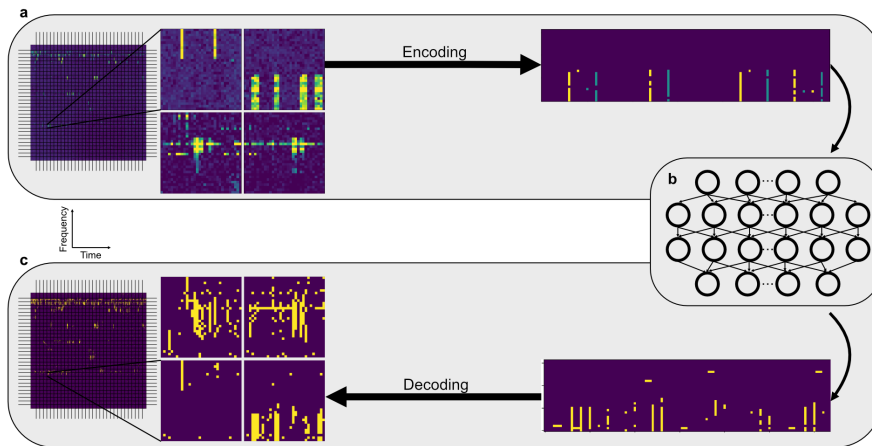


Fig. 1: SNN-Based RFI Detection Workflow. (a) Encoding: A spectrogram is divided into smaller patches and encoded into spikes using methods like delta-exposure encoding (shown with an exposure time of four). (b) SNN Processing: The encoded spikes are input into an SNN with a structure matching the spectrogram’s frequency channels. The SNN identifies RFI patterns from the time-varying data. (c) Decoding: Output spikes are decoded to produce an RFI mask for each patch, which is reassembled into a complete spectrogram RFI mask.

Encoding independent divisive normalisation

Divisive normalisation is an investigated and potentially canonical neural mechanism for filtering noisy signals in brains where the activity of a neuron is modulated by the summed activity of a pool of neighbouring neurons [23, 27]. Divisive normalisation has also been shown to play a role in choice behaviour [28]. Divisive normalisation has recently improved image segmentation performance in U-Net ANNs [24]. Knowing that most astronomical signals present as unstructured noise in a single spectrogram, we investigated applying some form of divisive normalisation to both datasets investigated. We additionally required a technique applied to any spike encoding and, as such, formulate a divisive normalisation-like preprocessing step. For visibility data $V(v, T, b)$, we define divisible normalised visibilities as:

$$V_{dn}(v, T, b) = V(v, T, b) - \sum_{i=-\frac{k}{2}}^{i=\frac{k}{2}} V(v+i, t-1, b) \quad (3)$$

where k is a configurable kernel size, in our case, three, $0 \leq v+i \leq 512$ and $T-1 \geq 0$; the bounds of the frequency channels and time in the original spectrogram. This

method effectively acts as a kernel over the localised frequency channels in the immediately preceding time step. We chose to include information from only a single previous time step to keep this method lightweight and plausible in a real-time collection setting. Figure 2 shows an example of this process acting on a LOFAR spectrogram with latency encoding. The visibly less noisy background retains most RFI features and results in significantly fewer spikes in the encoded spike train input, effectively increasing the information carried by each spike toward the goal of RFI detection.

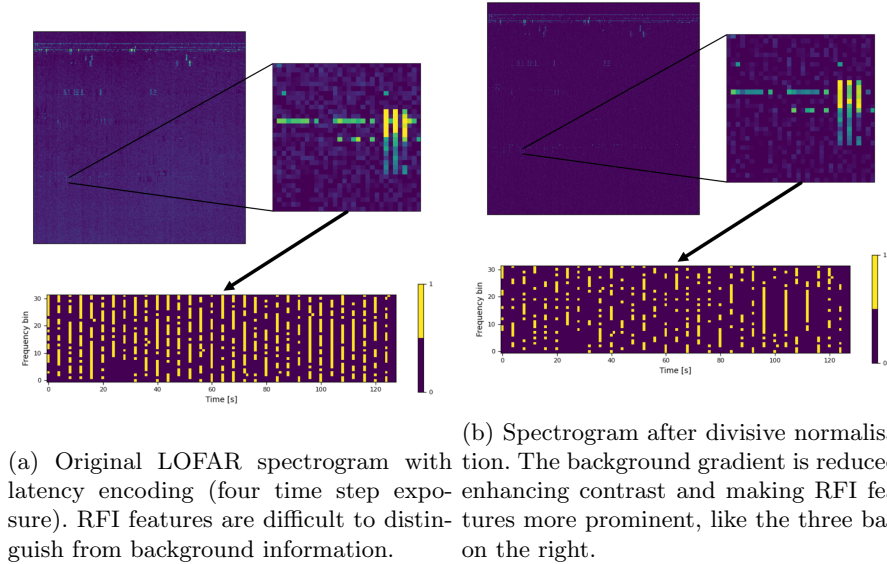


Fig. 2: Effects of divisive normalisation on spectrogram pre-processing for RFI detection.

Hyper-parameter tuning on synthetic HERA dataset

In addition to experimenting with different encoding methods, we wanted to experiment with network sizes and neuron parameters through hyper-parameter optimisation. The HERA dataset, while artificial, contains simulated RFI sources that reflect real-world sources. Full details of this dataset are available in the methods section. For all trials, we measure the Area Under the Receiver Operating Characteristic curve (AUROC), the Area Under the Precision-Recall Curve (AUPRC), per-pixel Accuracy, and the F1-Score. The definitions and significance of these values are found in the methods section. Owing to the relatively low per-pixel prevalence of RFI in both datasets, we expect high accuracy and AUROC values but pay greater attention to AUPRC and F1-Score, class-balanced performance measures. Our previous investigation into encoding methods tuned a restricted set of parameters, fixing the network

architecture but varying batch size and training epochs. We subsequently validated the parameters discovered with repeat trials and presented the results at an earlier conference venue [25]. These results with additional results containing replicated experiments with the new delta-exposure encoding are available in the supplementary information section, but we will summarise our findings below. We found our SNN approach to outperform equivalent ANN networks, and informed our decision to focus on delta-exposure, latency and step-forward direct encodings in the new work presented in this article.

Here, we present results from the search through additional network shaping parameters like layer depth and width and spiking neuron parameters. The methods section contains full details of the parameter space searched. Table 1 contains results from our hyper-parameter search exploring network parameters for delta-exposure, latency and step-forward-direct encoding method with and without divisive normalisation on the synthetic HERA dataset. We find that latency encoding with divisive normalisation performs best in all metrics except AUROC, which is narrowly beaten out by a raw ANN with divisive normalisation. The optimiser generally favoured larger than 128-sized hidden layers and increased network depth. Delta exposure encoding favoured higher beta values and larger exposure times, indicating a preference for fast decaying neurons, with latency and step-forward encodings preferring shorter exposure times and slower decaying neurons.

Table 1: Hyper-parameter search using Optuna multi-variate optimisation for the synthetic HERA dataset.

Encoding Method	Accuracy	AUROC	AUPRC	F1-Score	Num Hidden	Num Layers	Beta	Exposure
Delta-Exposure								
	0.990	0.864	0.791	0.764	512	3	0.435	53
	0.990	0.885	0.787	0.767	512	4	0.621	54
	0.981	0.888	0.672	0.628	512	4	0.731	24
	0.990	0.870	0.786	0.767	256	5	0.704	35
Delta-Exposure + DN								
	0.990	0.869	0.787	0.764	512	4	0.525	21
	0.989	0.874	0.751	0.733	512	4	0.747	22
Latency								
	0.982	0.929	0.736	0.691	128	6	0.246	10
	0.978	0.905	0.732	0.692	256	3	0.010	4
<u>Latency + DN</u>								
	0.998	0.969	0.945	0.942	256	5	0.239	4
Step-Forward-Direct								
	0.986	0.877	0.733	0.717	512	6	0.102	9
Step-Forward-Direct + DN								
	0.989	0.940	0.802	0.780	512	6	0.246	37
	0.990	0.918	0.836	0.827	256	5	0.025	33
ANN								
	0.984	0.929	0.823	0.800	128	2	-	-
	0.977	0.958	0.778	0.694	256	3	-	-
ANN + DN								
	0.994	0.976	0.922	0.914	512	3	-	-
	0.993	0.977	0.902	0.887	512	5	-	-
	0.994	0.976	0.921	0.914	512	3	-	-

We show the trials that performed best in at least one metric per encoding method. Best scores are in bold. Divisive Normalisation abbreviated to 'DN'. 'Num Hidden' refers to the number of neurons in each hidden layer, and 'Num Layers' refers to the number of hidden layers. The best overall encoding method is underlined. Each entry scored the highest in at least one performance measure, hence the variable number of entries per encoding method.

Effects of divisive normalisation on synthetic HERA dataset

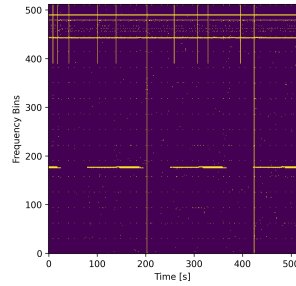
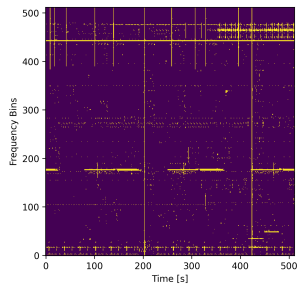
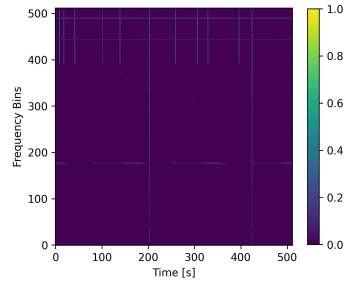
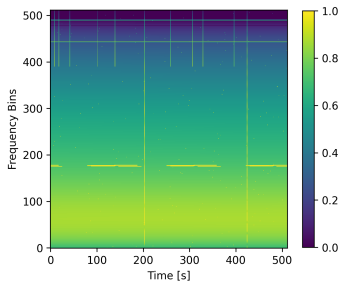
We took the best-performing trials as described in the methods section for each method and performed ten repeat trials to verify the performance of each. Table 2 contains the results of these trials. As in hyper-parameter optimisation, latency encoding with divisive normalisation performs strongest, followed by ANN networks with divisive normalisation.

Table 2: The final results show the performance of each encoding method using the final hyper-parameters on the HERA dataset.

Encoding Method	Accuracy		AUROC		AUPRC		F1	
Delta Exposure	0.984	0.006	0.869	0.004	0.699	0.051	0.671	0.065
Delta Exposure + DN	0.986	0.002	0.716	0.022	0.867	0.002	0.692	0.025
Latency	0.974	0.004	0.570	0.029	0.816	0.005	0.541	0.039
Latency + DN	0.996	0.002	0.968	0.001	0.914	0.034	0.907	0.042
Step-Forward-Direct	0.709	0.018	0.984	0.001	0.878	0.004	0.687	0.023
Step-Forward-Direct + DN	0.990	0.002	0.823	0.037	0.936	0.001	0.805	0.046
ANN	0.879	0.067	0.645	0.079	0.894	0.031	0.440	0.155
ANN + DN	0.993	0.001	0.901	0.016	0.976	0.001	0.886	0.023

Each metric is listed as mean and standard deviation. Ten trials were completed for each encoding method. Divisive Normalisation abbreviated to ‘DN’. The best scores are bolded. Latency encoding with divisive normalisation offers superior performance in two metrics. Divisive normalisation significantly improves accuracy, AUPRC, and F1 scores for all methods while degrading AUROC scores slightly for the delta-exposure and step-forward-direct encodings.

Figure 3 presents an example spectrogram original and divisible normalised, latency encoded inference, and the original ground-truth RFI mask. This figure clearly shows that divisive normalisation removes almost all of the background ‘gradient’ information representing the simulated astronomical background from the dataset, resulting in significantly clearer inputs and outputs from the SNN. On average, divisive normalisation improved accuracy by 0.102, AUROC by 0.029, AUPRC by 0.108 and F1-Score by 0.168 across each spike-encoding method. We find latency encoding with divisive normalisation to be the strongest performing encoding method with an AUROC of 0.968, AUPRC of 0.914 and F1-Score of 0.907 to be comparable with state-of-the-art traditional algorithms, ANN methods and ANN2SNN conversions on this dataset. Specifically, the best-reported performance using AOFlagger [8], an operational RFI flagging scheme achieves an AUROC of 0.973, AUPRC of 0.880 and F1-Score of 0.873 [14]. The best reported ANN method [15] achieves an AUROC of 0.994, AUPRC of 0.959 and F1-Score of 0.945. Finally, the best previous SNN method, Spiking-Nearest-Latent-Neighbours (SNLN) [20] achieves an AUROC of 0.944, AUPRC of 0.920 and F1-Score of 0.953. SNLN, while performant, is computationally intensive, using a much larger network architecture and long inference times. We, therefore, claim that our method is near state-of-the-art despite significantly lower computational requirements than other comparable methods.



(c) Latency-based inference on the original spectrogram.

(d) Latency-based inference on the normalised spectrogram shows clearer RFI features.

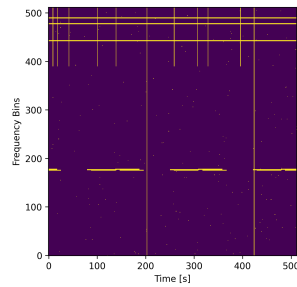


Fig. 3: Impact of Divisive Normalisation on RFI Detection in HERA Spectrograms. Divisive normalisation significantly reduces background noise while preserving key RFI features, improving inference performance of the SNN.

Hyper-parameter tuning on real LOFAR dataset

We optimised hyper-parameters on a real LOFAR-derived dataset with the same methodology as the synthetic HERA dataset. The methods section contains full details of this realistic dataset. Being based in population-dense Europe, the RFI environment of this instrument is significantly more challenging than in the synthetic dataset. Table 3 contains results from our hyper-parameter search on the real LOFAR dataset. We find performance across the board degraded significantly compared to the synthetic case where the ANN with and without divisive normalisation performs best in a single trial. The optimiser favours slightly shallower networks with faster decay rates, wider hidden layers and longer exposure times across all encoding methods.

Table 3: Hyper-parameter search using Optuna multi-variate optimisation for the real LOFAR dataset.

Encoding Method	Accuracy	AUROC	AUPRC	F1-Score	Batch Size	Epochs	Beta	Exposure
Delta-Exposure								
	0.975	0.568	0.163	0.127	512	2	0.736	57
	0.988	0.539	0.158	0.146	128	2	0.162	18
	0.986	0.561	0.173	0.158	512	5	0.374	62
Delta-Exposure + DN								
	0.986	0.514	0.100	0.093	256	5	0.840	11
	0.970	0.563	0.152	0.111	512	2	0.735	55
	0.974	0.551	0.141	0.114	512	3	0.742	23
Latency								
	0.988	0.568	0.248	0.211	512	2	0.149	61
	0.977	0.610	0.226	0.175	512	2	0.592	52
Latency + DN								
	0.981	0.617	0.240	0.198	512	3	0.418	63
	0.976	0.628	0.244	0.184	256	2	0.675	62
	0.989	0.550	0.218	0.188	512	5	0.109	23
Step-Forward-Direct								
	0.970	0.636	0.247	0.171	512	2	0.441	29
	0.986	0.624	0.283	0.246	512	2	0.512	24
Step-Forward-Direct + DN								
	0.971	0.628	0.238	0.167	512	3	0.263	42
	0.968	0.633	0.241	0.162	512	4	0.373	30
	0.973	0.583	0.183	0.140	512	6	0.078	62
<u>ANN</u>								
	0.992	0.485	0.519	0.047	512	6	-	-
	0.977	0.761	0.450	0.356	512	3	-	-
	0.976	0.765	0.451	0.351	512	3	-	-
ANN + DN								
	0.674	0.673	0.403	0.114	512	4	-	-
	0.719	0.689	0.389	0.090	256	2	-	-
	0.992	0.485	0.519	0.047	512	6	-	-

We show the trials that performed best in at least one metric per encoding method. The best scores are in bold. Divisive Normalisation abbreviated to 'DN'. 'Num Hidden' refers to the number of neurons in each hidden layer, and 'Num Layers' refers to the number of hidden layers. The best overall encoding method is underlined. Each entry scored the highest in at least one performance measure, hence the variable number of entries per encoding method.

Effects of divisive normalisation on real LOFAR dataset

In line with our approach to the HERA dataset, we took the best-performing parameters for each method and performed repeat trials to verify performance. Table 4 contains the results of these trials. We see that, on aggregate, our SNN-encoded methods perform better than the equivalently sized ANN methods. The best-performing method overall is Step-forward encoding with direct exposure; however, the significantly better AUROC score from latency encoding with divisive normalisation is noteworthy.

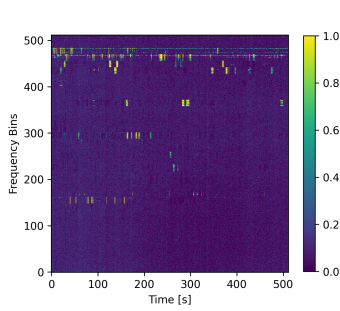
Table 4: The final results show the performance of each encoding method using the final hyper-parameters on the LOFAR dataset.

Encoding Method	Accuracy		AUROC		AUPRC		F1	
Delta Exposure	0.973	0.007	0.149	0.009	0.556	0.002	0.120	0.017
Delta Exposure + DN	0.961	0.005	0.143	0.004	0.555	0.003	0.097	0.006
Latency	0.972	0.017	0.190	0.037	0.566	0.004	0.149	0.042
Latency + DN	0.978	0.003	0.630	0.003	0.254	0.011	0.198	0.016
Step-Forward-Direct	0.983	0.002	0.262	0.011	0.628	0.005	0.217	0.014
Step-Forward-Direct + DN	0.945	0.011	0.218	0.014	0.613	0.015	0.128	0.011
ANN	0.748	0.165	0.439	0.053	0.608	0.083	0.087	0.027
ANN + DN	0.862	0.160	0.473	0.056	0.559	0.091	0.072	0.032

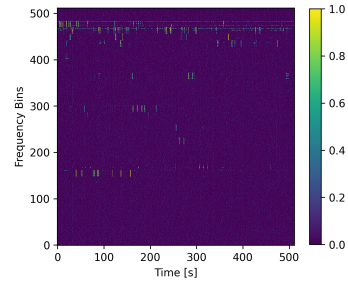
Each metric is listed as mean and standard deviation. The best scores are bolded. Ten trials were completed for each encoding method. Divisive Normalisation abbreviated to ‘DN’. Step-forward-direct encoding without divisive normalisation offers the best overall performance in accuracy, AUPRC, and F1 scores. Latency encoding with divisive normalisation offers significantly higher AUROC performance than all other methods.

In Figure 4, the SNN outputs are noisy with or without divisive normalisation, although the inference trained on normalised data shows the RFI features more prominently. Interestingly, there appears to be subtle banding in the outputs of Figures 4c (horizontal) and 4d (vertical), the difference in orientation suggests perhaps a tendency for the networks to present a bias towards frequency isolated or time-isolated RFI respectively. While promising, the noisy output of the SNN is likely contributing to a degraded performance. On average, divisive normalisation degraded accuracy by 0.015, AUPRC by 0.109 and F1-Score by 0.021 but improved AUROC by 0.130 across each spike-encoding method. We find Step-forward-direct encoding to give the strongest performance with an AUROC of 0.262, AUPRC of 0.628, and F1-Score of 0.217. These results are compelling for such relatively lightweight architectures, however there exists a gap to the state-of-the-art. The best reported AOFlogger [8] results [14] give an AUROC of 0.788, AUPRC of 0.572 and F1-Score of 0.570. The best reported F1-score for an ANN method on this dataset is 0.742 [17]. The best reported AUROC and AUPRC values for an ANN method, Remove First Detect Later (RFDL), on this dataset are 0.989 and 0.748, respectively, and the best reported F1-score for the RFDL method is 0.660 [15]. Finally, the best ANN2SNN conversion achieves an AUROC of 0.609, AUPRC of 0.321 and F1-Score of 0.408 [20]. We additionally note that our best AUROC score from latency encoding with divisive normalisation achieves an AUROC of 0.630. These results indicate there exists potential for our time-series

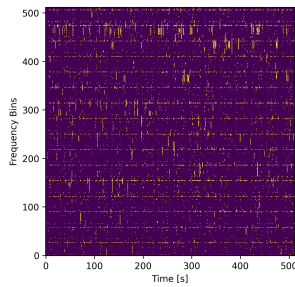
segmentation approach applied to real astronomical data, however some additional developments are needed to close the gap to the state-of-the-art.



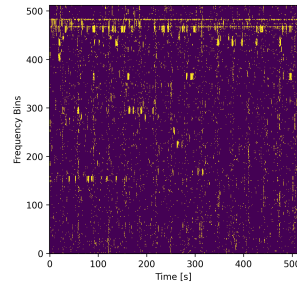
(a) Original spectrogram.



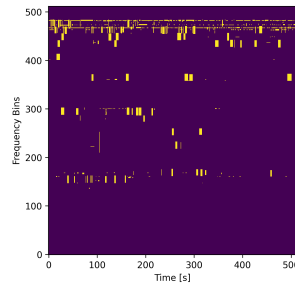
(b) Spectrogram after divisive normalisation.



(c) Latency-based inference on the original spectrogram.



(d) Latency-based inference on the normalised spectrogram shows clearer RFI detection.



(e) Expert-labelled RFI mask.

Fig. 4: Impact of Divisive Normalisation on RFI Detection in LOFAR Spectrograms. While divisive normalisation improves clarity, the SNN output still exhibits some noise compared to expert labelling.

Discussion

This study demonstrates that SNNs can effectively perform time-series segmentation tasks, specifically RFI detection in radio astronomy. Reformulating RFI detection as a time-series segmentation problem, we leveraged the temporal dynamics inherent to spiking neurons to recognise complex patterns. We explored various spike encoding methods, including latency, rate, delta-modulation, delta-exposure and step-forward encodings to convert ‘visibility’ spectrographic data to spikes. We additionally explored optimising network depth and hidden layer widths alongside the spiking neuron and encoding parameters. Our experiments show that simple feed-forward SNNs of first-order leaky-integrate-and-fire neurons perform well on synthetic datasets, achieving near state-of-the-art results and moderately well on real-world data from the LOFAR instrument, despite increased noise and variability, outperforming equivalent ANNs. To our knowledge, this work is the first to train SNNs on a real radio astronomy observation dataset successfully. Our findings suggest latency with divisive normalisation and step-forward (direct exposure) encoding methods performed particularly well. This indicates that SNNs may tolerate several different spike encoding schemes.

A key contribution of this work is introducing a divisive normalisation-inspired pre-processing step. Our results indicate that this pre-processing can significantly improve detection performance, particularly on the synthetic dataset. However, expanding the normalisation kernel size or incorporating information from additional prior time steps may further improve performance on realistic datasets, where background information is more dynamic.

Despite promising initial results, our work has limitations. Training resources on the LOFAR dataset were equivalent to the synthetic HERA dataset; training for extended durations with larger networks may provide additional performance. Directly scaling this work’s methods is yet to be exhausted. Still, the combination of increased computational requirements in simulating large SNNs and the wider configurability of spiking neurons makes exploring this space particularly challenging. Further developments on both the data-preparation and architectural fronts may provide additional performance. For example, capturing the polarity information from the original observational data, developing more sophisticated architectures that consume entire spectrograms in a multi-headed approach or with built-in de-noising capabilities and exploring training encodings are of future interest. Future work could also focus on integrating more sophisticated neuron models, such as sigma-delta or second-order LiF neurons, decoding the generally noisy output spike-trains in a trainable fashion, or casting other spectrographic segmentation tasks as time-series segmentation, such as oceanography or seismic inversion.

Modern radio astronomy is as much a science based on building precision instruments as high-performance computing. Over multi-decade project horizons, integrating cutting-edge computing methods to find performance and efficiency benefits directly translates into greater scientific impact over the life of a telescope. Despite this work’s promising first steps, challenges remain regarding the operational integration of neuromorphic computing into radio astronomy processing. While access to commercial nascent neuromorphic hardware has never been easier, most platforms

focus primarily on image-oriented [29, 30] or narrow-width time-series inputs (relative to the needs of radio astronomy) [31]. Platforms like Intel’s Loihi [29, 32] provide greater flexibility, but the practical performance and efficiency of such systems on RFI detection is yet to be known. Moreover, many focus on edge-computing use cases, where small size, weight and power consumption dominate design considerations. In an observatory environment, the opportunity exists to target physically larger, more powerful neuromorphic systems that still provide energy efficiencies relative to contemporary high-performance computing systems. Moreover, a practical claim of RFI detection techniques suitable for real-time processing demands rigorous performance analysis that may impose strict requirements on exposure times, for example, when considering the time-series segmentation method this article presents. Integrating neuromorphic computing into radio astronomy or other data-intensive sciences could be a prime candidate for hardware-software co-design. Finally, there exists the challenge, not unique to potential SNN-based methods, of integrating machine-learned or automated methods, which can be brittle and difficult to adapt quickly, into operational observatories generally.

In conclusion, our investigation continues to pave the way for applying SNNs and neuromorphic computing in radio astronomy, offering unique advantages over contemporary methods. We contribute to advancing efficient, adaptive data processing techniques essential to the future of radio astronomy while simultaneously finding a new domain to explore the capabilities of neuromorphic computing and SNNs.

Methods

HERA Dataset

The synthetic dataset Mesarcik et al. [14] describe fully comes from the Hydrogen Epoch of Reionisation Array (HERA) simulator [33]. This dataset contains 420 training spectrograms and 140 test spectrograms. Each spectrogram covers a 30-minute simulation integrating every 3.52 seconds (producing 512 time steps) and 512 frequency channels from 105MHz to 195MHz. The RFI is synthetic but modelled from satellite communications (localised in frequency, covering all time), lightning (covering all frequencies, localised in time), ground communication (localised in frequency, partially localised in time), and impulse blips (localised in frequency and time). Overall, per-pixel RFI contamination sits at 2.76%.

LOFAR Dataset

The LOFAR dataset, as fully described by Mesracik et al. [14], consists of 7,500 training spectrograms with corresponding masks produced by AOflogger [8], along with 109 testing spectrograms that have been expertly hand-labelled. This dataset originates from five observations, totalling 1.7 TB in size. To reduce this volume, the dataset was downsampled by selecting only the first Stokes parameter and randomly sampling 1,500 baselines, resulting in a more manageable size of approximately 10 GB. Combining machine-generated labels and hand-labelled testing examples adds to the complexity and challenge of the dataset in addition to a significantly more difficult

noise environment. We trained on 15% of the training samples for our experiments, 1125 spectrograms.

SNN neuron model

This work utilises a first-order leaky integrate and fire neuron model reset with subtraction, found in `snnTorch` [34]. The linear differential equation modelling the membrane potential $U(t)$ dynamics of a single neuron subject to an input current I_{in} is given as:

$$\tau \frac{dU(t)}{dt} = -U(t) + I_{in}(t)R, \quad (4)$$

where $\tau = RC$ is a fixed time constant. In practice, the recurrent behaviours of the neuron are given as follows:

$$U[t + 1] = \beta U[t] + I_{in}[t + 1] - RU_{thr}, \quad (5)$$

where β is a tunable decay-rate parameter, U_{thr} is the neuron’s membrane threshold, and R is a gating parameter subtracting the threshold potential if a spike is emitted in the previous time step.

Simulation environment

All simulations were conducted on the Setonix supercomputer, an HPE Cray EX system located at the Pawsey Supercomputing Centre in Western Australia. Specifically, each trial utilised a single node with a single AMD EPYC 7A53 ‘Trento’ 64-core CPU, eight AMD Instinct MI250X GPUs, and 256 GB of RAM. For SNN network training, we employed the `snnTorch` framework [34], with distributed training managed by the Lightning library [35] to efficiently leverage the available GPU resources.

Hyper-Parameter tuning details

We use the tree-structured Parzan estimation algorithm Optuna [36] exposes for multi-variate optimisation. We simultaneously optimised for per-pixel accuracy, Area Under the Receiver Operating Characteristic curve (AUROC), Area Under the Precision-Recall Curve (AUPRC), Accuracy, and F1-Score. AUROC evaluates the ratio of True Positive Rate (TPR) and False Positive Rate (FPR) across all possible classification thresholds. AUPRC gives the ratio of precision and recall across several thresholds, in this case referring to the proportion of correctly classified RFI over all RFI predictions. Recall, in this case, is the TPR. Accuracy is the per-pixel output accuracy. We expect accuracy to be very high for both the synthetic and real radio astronomy datasets as true RFI flags are very sparse; a completely silent network would still be more than 90% accurate. F1-Score is the harmonic mean of precision and recall at a given threshold. The sparsity of RFI in this dataset means we generally expect high AUROC and high accuracy values with lower AUPRC and F1 scores. A good-performing model must be silent most of the time while providing confident RFI detections, hence our inclusion of both raw accuracy and F1-scores. Results for each trial were uploaded to

a persistent database from which Optuna read, allowing each trial to execute as an individual job. Each hyper-parameter trial ran for 50 epochs with an initial learning rate of $1e - 3$. However, utilising Lightning’s plateau scheduler reduced the learning rate by half for every ten epochs with no improvement in validation loss. Batch size for all trials was fixed at 36. Table 5 contains the ranges and descriptions of each hyper-parameter tuned for each encoding. In Table 5, ‘Num hidden’ refers to the number of neurons in each hidden layer. ‘Num layers’ refers to the number of hidden layers in the network. Beta defines the excitability of LiF neurons within the network, and exposure is a parameter for the encoding method used in all but the delta-modulation method. Beta and exposure hold no meaning for ANN networks and are omitted for these trials. For all encoding methods, we took the trial with the highest-scoring results in the most categories into repeated trials, tie-breaking by F1-Score performance.

Table 5: Parameter ranges for attributes included in the final hyper-parameter searches.

Attribute	Parameter Range
Num Hidden	128, 256, 512
Num Layers	2 - 6
Beta	0.5 - 0.99
Exposure	1 - 64

Repeat trial simulation details

Repeat trial simulations were run for 100 epochs, each with the same learning rate scheduling and batch size as the hyper-parameter trials.

Spike Encoding Methods

Each encoding method involves a spike-encoding scheme, decoding scheme and loss function. Figure 5 contains example plots for all encodings with a sample spectrogram exposed for four time steps where applicable. As mentioned previously, these encoding methods take a set of ‘visibilities’ $V(v, T, b)$ and output a spike-train with dimensions $V(v, T \cdot E, b)$ where E is an integer exposure time.

Latency

Our latency encoding scheme is relatively straightforward. For a given exposure E , input pixel intensities are mapped inversely linearly from 0 to E , meaning high-intensity pixels spike almost immediately and low-intensity pixels progressively later.

For output decoding, we interpret any spikes before the last exposure step as an RFI mask and no spikes or a spike in the final exposure as background. The following

equation maps the spike times in the supervised masks, that is, the t value in $F(v, t, b)$:

$$t = \begin{cases} 0 & G(v, t, b) = 1 \\ E & otherwise \end{cases} \quad (6)$$

The comparison function, \mathcal{H} , is the mean square spike time governed by the following function:

$$\mathcal{H}_{latency} = \sum_e^E \sum_v^V (y_{v,e} - f_{v,e})^2. \quad (7)$$

Figure 5b contains an example input raster plot.

Rate

Rate encoding is well-understood and widely used when processing image data in SNNs. For a given exposure E , we interpret pixel values as firing probabilities. We map supervised masks to firing rates of 0.8 for pixels labelled as containing RFI and 0.2 for pixels that do not. For output decoding, we interpret outputs with a firing rate greater than 0.75 as an RFI flag.

To map rate-encoding into a time-series segmentation problem, we treat each time step in the original signal as a classification problem. The comparison function, \mathcal{H} , is an adjusted mean square error spike count loss, adapted from the implementation in `snnTorch` [34] to handle time segments with no positive labels present, and is governed by the following equation:

$$\mathcal{H}_{rate} = \sum_e^E (y_{v,e} - f_{v,e})^2. \quad (8)$$

Figure 5c contains an example input raster plot.

Delta-Modulation

Delta-modulation encoding encodes inputs only on relative change. Our method utilises the delta-modulation encoding method in `snnTorch` [34], using both positive and negative polarity spikes. Output decoding is a more complex procedure. Encoding regions of an RFI mask that can span as little as a single pixel requires spike polarity for ‘on’ and ‘off’ spikes. However, in our networks, neurons only emit positive spikes. Therefore, we double the frequency width of the output layer and move all negative polarity spikes to the lower region as positive spikes.

The comparison function, \mathcal{H} , is the Huber loss function, which combines L1 and MSE loss functions, computing the squared MSE term if the error falls below a threshold and L1 loss otherwise. We employ this loss function to handle the sparsity of the output spike trains. The Huber loss as acting on spike-trains is:

$$\mathcal{H}_{delta} = \begin{cases} \frac{1}{2}(y - f)^2 & |y - f| \leq \delta \\ \delta(|y - f| - \frac{1}{2}\delta) & otherwise \end{cases} \quad (9)$$

Figure 5d contains an example input raster plot.

Delta-Exposure

Delta exposure is a hybrid of the latency and delta-modulation methods. Input encoding is similar to delta modulation. However, we include an exposure time to give the network more time to react to the input stimulus. Output decoding is also simplified to the scheme described in equation 7. Figure 5e contains an example raster for this scheme.

Step-Forward

Visibility data is spatio-temporal, so we tested encoding methods based on encoding audio data, the Step-Forward algorithm [21]. This approach takes the step-wise difference between the signal at each time step and a running cumulative sum, emitting a positive or negative spike when the difference crosses a threshold (in our case, 0.1) upwards or downwards. Additionally, a cumulative sum of these differences is appended to the end of the frequency channels, doubling the width of the input. Output decoding and supervised mask encoding, covered in Equation 6, are handled identically to latency encoding. The comparison function is also identical to latency encoding, covered in Equation 7. We provide three methods to adapt the original step-forward algorithm to the time-series segmentation problem outlined below; each method handles the required exposure parameter.

First

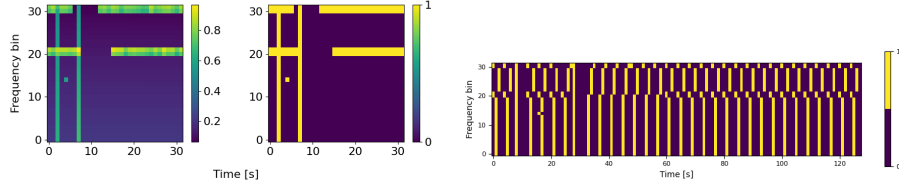
This exposure mode presents spikes to the network only on the first exposure step for each time step, with silence following. Figure 5f contains an example raster plot for this exposure method.

Direct

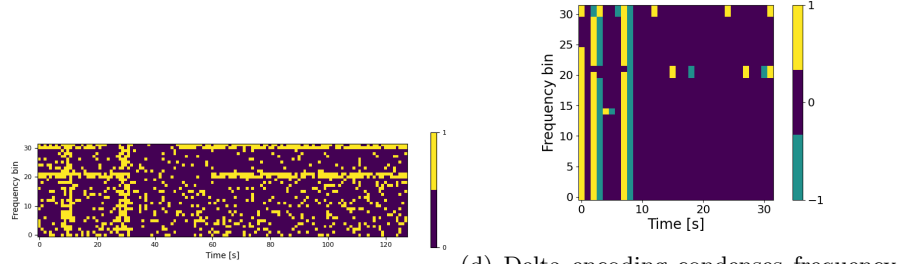
This exposure mode presents spikes to the network at every exposure step for each time step. Figure 5g contains an example raster plot for this exposure method.

Latency

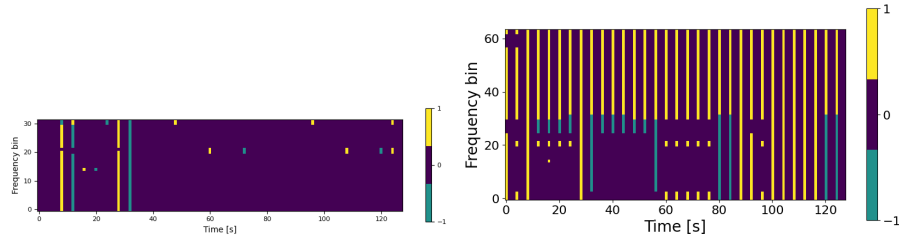
This exposure mode presents spikes to the network latency encoded at exposure time 0 where a spike is present and exposure time E otherwise. Figure 5h contains an example raster plot for this exposure method.



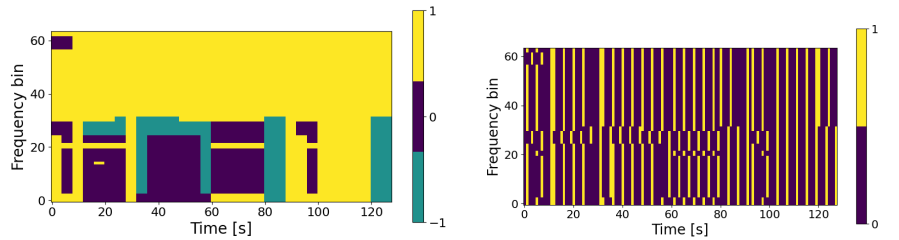
(a) The original input spectrogram and (b) Latency encoding reveals clear banding and associated RFI mask.



(c) Rate encoding reveals most features clearly but struggles with isolated blips. (d) Delta encoding condenses frequency-isolated RFI into a few spikes, making thresholding during encoding critical.



(e) Delta exposure encoding improves but still struggles with frequency-isolated RFI. (f) Step-Forward encoding with 'first' exposure mode clearly shows banding but is hard to interpret.



(g) Step-Forward encoding with 'direct' exposure is active but shows the difficulty in identifying bands. (h) Step-Forward encoding example with 'latency' exposure effectively identifies bands and blips.

Fig. 5: Spike Raster Plots for Various Encodings Applied to Synthetic HERA Data. Encodings are exposed for four time steps where applicable, showcasing how different methods capture distinct RFI features.

Data availability

This study's datasets are openly available online [37].

Code availability

Source code is openly available [38].

References

- [1] Trappenberg, T.P.: Fundamentals of Computational Neuroscience, 2nd ed. edn. Oxford University Press, Oxford, UK ; (2010). Publication Title: Fundamentals of computational neuroscience
- [2] Ottati, F., Gao, C., Chen, Q., Brignone, G., Casu, M.R., Eshraghian, J.K., Lavagno, L.: To Spike or Not To Spike: A Digital Hardware Perspective on Deep Learning Acceleration. *IEEE Journal on Emerging and Selected Topics in Circuits and Systems*, 1–1 (2023) <https://doi.org/10.1109/JETCAS.2023.3330432> . Conference Name: IEEE Journal on Emerging and Selected Topics in Circuits and Systems
- [3] Schuman, C.D., Kulkarni, S.R., Parsa, M., Mitchell, J.P., Date, P., Kay, B.: Opportunities for neuromorphic computing algorithms and applications. *Nature Computational Science* **2**(1), 10–19 (2022) <https://doi.org/10.1038/s43588-021-00184-y> . Number: 1 Publisher: Nature Publishing Group
- [4] Vermij, E., Fiorin, L., Jongerius, R., Hagleitner, C., Bertels, K.: Challenges in exascale radio astronomy: Can the SKA ride the technology wave? *The International Journal of High Performance Computing Applications* **29**(1), 37–50 (2015) <https://doi.org/10.1177/1094342014549059> . Publisher: SAGE Publications Ltd STM
- [5] IAU Statement on Satellite Constellations (2019). <https://www.iau.org/news/announcements/detail/ann19035/>
- [6] Statement on Starlink and 'Constellations' of Communication Satellites (2019). <https://192.33.115.60/news/nrao-statement-commsats/>
- [7] Report of the Committee on the Peaceful Uses of Outer Space. Technical Report 65, United Nations Office for Outer Space Affairs (August 2022). https://www.unoosa.org/oosa/oosadoc/data/documents/2022/a/a7720_0.html
- [8] Offringa, A.: AOflogger: RFI Software. Astrophysics Source Code Library, 1010 (2010)
- [9] Perez-Portero, A., Querol, J., Camps, A., Martin-Neira, M., Suess, M., Ramirez,

- J.I., Zurita, A., Closa, J., Oliva, R., Onrubia, R.: RFI Detection and Mitigation for Advanced Correlators in Interferometric Radiometers. *Remote Sensing* **14**(18), 4672 (2022) <https://doi.org/10.3390/rs14184672> . Number: 18 Publisher: Multidisciplinary Digital Publishing Institute
- [10] Mohamed-Fakier, Z., Paine, S., Winberg, S.: Transient Radio Frequency Interference Detection Using MeerKAT’s D-Engine. In: 2024 4th URSI Atlantic Radio Science Meeting (AT-RASC), pp. 1–5 (2024). <https://doi.org/10.46620/URSIATRASC24/BUTR1006> . <https://ieeexplore.ieee.org/abstract/document/10584605>
- [11] Akeret, J., Chang, C., Lucchi, A., Refregier, A.: Radio frequency interference mitigation using deep convolutional neural networks. *Astronomy and Computing* **18**, 35–39 (2017) <https://doi.org/10.1016/j.ascom.2017.01.002>
- [12] Vafaei Sadr, A., Bassett, B.A., Oozeer, N., Fantaye, Y., Finlay, C.: Deep learning improves identification of Radio Frequency Interference. *Monthly Notices of the Royal Astronomical Society* **499**(1), 379–390 (2020) <https://doi.org/10.1093/mnras/staa2724>
- [13] Yang, Z., Yu, C., Xiao, J., Zhang, B.: Deep residual detection of radio frequency interference for FAST. *Monthly Notices of the Royal Astronomical Society* **492**(1), 1421–1431 (2020) <https://doi.org/10.1093/mnras/stz3521>
- [14] Mesarcik, M., Boonstra, A.-J., Rangelova, E., van Nieuwpoort, R.V.: Learning to detect radio frequency interference in radio astronomy without seeing it. *Monthly Notices of the Royal Astronomical Society* **516**(4), 5367–5378 (2022) <https://doi.org/10.1093/mnras/stac2503>
- [15] van Zyl, D.J., Grobler, T.L.: Remove First Detect Later: a counter-intuitive approach for detecting radio frequency interference in radio sky imagery. *Monthly Notices of the Royal Astronomical Society* **530**(2), 1907–1920 (2024) <https://doi.org/10.1093/mnras/stae979>
- [16] Ouyang, X., Dreuning, H., Mesarcik, M., Nieuwpoort, R.V.: Hierarchical vision transformers for RFI mitigation in radio astronomy, Bariloche, Argentina (2024)
- [17] Du Toit, C.D., Grobler, T.L., Ludick, D.J.: A comparison framework for deep learning RFI detection algorithms. *Monthly Notices of the Royal Astronomical Society* **530**(1), 613–629 (2024) <https://doi.org/10.1093/mnras/stae892>
- [18] Kasabov, N., Scott, N.M., Tu, E., Marks, S., Sengupta, N., Capecci, E., Othman, M., Doborjeh, M.G., Murli, N., Hartono, R., Espinosa-Ramos, J.I., Zhou, L., Alvi, F.B., Wang, G., Taylor, D., Feigin, V., Gulyaev, S., Mahmoud, M., Hou, Z.-G., Yang, J.: Evolving spatio-temporal data machines based on the NeuCube neuromorphic framework: Design methodology and selected applications. *Neural Networks* **78**, 1–14 (2016) <https://doi.org/10.1016/j.neunet.2015.09.011>

- [19] Scott, N.M.: Evolving Spiking Neural Networks for Spatio- and Spectro- Temporal Data Analysis: Models, Implementations, Applications. PhD thesis, Auckland University of Technology (2015). <https://hdl.handle.net/10292/10601>
- [20] Pritchard, N.J., Wicenc, A., Bennamoun, M., Dodson, R.: RFI Detection with Spiking Neural Networks. Publications of the Astronomical Society of Australia, 1–11 (2024) <https://doi.org/10.1017/pasa.2024.27>
- [21] Stewart, K.M., Shea, T., Pacik-Nelson, N., Gallo, E., Danielescu, A.: Speech2Spikes: Efficient Audio Encoding Pipeline for Real-time Neuromorphic Systems. In: Proceedings of the 2023 Annual Neuro-Inspired Computational Elements Conference. NICE '23, pp. 71–78. Association for Computing Machinery, New York, NY, USA (2023). <https://doi.org/10.1145/3584954.3584995> . <https://dl.acm.org/doi/10.1145/3584954.3584995>
- [22] Bos, H., Muir, D.: Sub-mW Neuromorphic SNN audio processing applications with Rockpool and Xylo. arXiv. arXiv:2208.12991 (2022). <https://doi.org/10.48550/arXiv.2208.12991> . <http://arxiv.org/abs/2208.12991>
- [23] Carandini, M., Heeger, D.J., Movshon, J.A.: Linearity and Normalization in Simple Cells of the Macaque Primary Visual Cortex. *The Journal of Neuroscience* **17**(21), 8621–8644 (1997) <https://doi.org/10.1523/JNEUROSCI.17-21-08621.1997>
- [24] Hernández-Cámara, P., Vila-Tomás, J., Laparra, V., Malo, J.: Neural networks with divisive normalization for image segmentation. *Pattern Recognition Letters* **173**, 64–71 (2023) <https://doi.org/10.1016/j.patrec.2023.07.017>
- [25] Pritchard, N.J., Wicenc, A., Bennamoun, M., Dodson, R.: Supervised Radio Frequency Interference Detection with SNNs. arXiv. arXiv:2406.06075 (2024). <https://doi.org/10.48550/arXiv.2406.06075> . <http://arxiv.org/abs/2406.06075>
- [26] Thompson, A.R., Moran, J.M., Swenson Jr., G.W.: Interferometry and Synthesis in Radio Astronomy, 3rd ed. 2017. edn. Astronomy and Astrophysics Library. Springer, Cham (2017). Publication Title: Interferometry and Synthesis in Radio Astronomy
- [27] Carandini, M., Heeger, D.J.: Normalization as a canonical neural computation. *Nature Reviews Neuroscience* **13**(1), 51–62 (2012) <https://doi.org/10.1038/nrn3136>
- [28] Webb, R., Glimcher, P.W., Louie, K.: Divisive normalization does influence decisions with multiple alternatives. *Nature Human Behaviour* **4**(11), 1118–1120 (2020) <https://doi.org/10.1038/s41562-020-00941-5>
- [29] Davies, M., Srinivasa, N., Lin, T.-H., China, G., Cao, Y., Choday, S.H., Dimou,

- G., Joshi, P., Imam, N., Jain, S., Liao, Y., Lin, C.-K., Lines, A., Liu, R., Mathaikutty, D., McCoy, S., Paul, A., Tse, J., Venkataramanan, G., Weng, Y.-H., Wild, A., Yang, Y., Wang, H.: Loihi: A Neuromorphic Manycore Processor with On-Chip Learning. *IEEE Micro* **38**(1), 82–99 (2018) <https://doi.org/10.1109/MM.2018.112130359> . Conference Name: IEEE Micro
- [30] Modha, D.S., Akopyan, F., Andreopoulos, A., Appuswamy, R., Arthur, J.V., Cassidy, A.S., Datta, P., DeBole, M.V., Esser, S.K., Otero, C.O., Sawada, J., Taba, B., Amir, A., Bablani, D., Carlson, P.J., Flickner, M.D., Gandhasri, R., Garreau, G.J., Ito, M., Klamo, J.L., Kusnitz, J.A., McClatchey, N.J., McKinstry, J.L., Nakamura, Y., Nayak, T.K., Risk, W.P., Schleupen, K., Shaw, B., Sivagnaname, J., Smith, D.F., Terrizzano, I., Ueda, T.: Neural inference at the frontier of energy, space, and time. *Science* **382**(6668), 329–335 (2023) <https://doi.org/10.1126/science.adh1174> . Publisher: American Association for the Advancement of Science
- [31] AG, S.: Xylo™: Ultra-low power neuromorphic chip | SynSense (2022). <https://www.synsense.ai/products/xylo/> Accessed 2024-08-22
- [32] Intel Advances Neuromorphic with Loihi 2, New Lava Software Framework. <https://www.intel.com/content/www/us/en/newsroom/news/intel-unveils-neuromorphic-loihi-2-lava-software.html> Accessed 2024-06-22
- [33] DeBoer, D.R., Parsons, A.R., Aguirre, J.E., Alexander, P., Ali, Z.S., Beardsley, A.P., Bernardi, G., Bowman, J.D., Bradley, R.F., Carilli, C.L., Cheng, C., Acedo, E.d.L., Dillon, J.S., Ewall-Wice, A., Fadana, G., Fagnoni, N., Fritz, R., Furlanetto, S.R., Glendenning, B., Greig, B., Grobbelaar, J., Hazelton, B.J., Hewitt, J.N., Hickish, J., Jacobs, D.C., Julius, A., Kariseb, M., Kohn, S.A., Lekalake, T., Liu, A., Loots, A., MacMahon, D., Malan, L., Malgas, C., Maree, M., Martinot, Z., Mathison, N., Matsetela, E., Mesinger, A., Morales, M.F., Neben, A.R., Patra, N., Pieterse, S., Pober, J.C., Razavi-Ghods, N., Ringuette, J., Robnett, J., Rosie, K., Sell, R., Smith, C., Syce, A., Tegmark, M., Thyagarajan, N., Williams, P.K.G., Zheng, H.: Hydrogen Epoch of Reionization Array (HERA). *Publications of the Astronomical Society of the Pacific* **129**(974), 045001 (2017) <https://doi.org/10.1088/1538-3873/129/974/045001> . Publisher: The Astronomical Society of the Pacific
- [34] Eshraghian, J.K., Ward, M., Neftci, E., Wang, X., Lenz, G., Dwivedi, G., Benamoun, M., Jeong, D.S., Lu, W.D.: Training spiking neural networks using lessons from deep learning. *Proceedings of the IEEE* **111**(9), 1016–1054 (2023)
- [35] Falcon, W., The PyTorch Lightning team: PyTorch Lightning (2019). <https://doi.org/10.5281/zenodo.3828935> . <https://github.com/Lightning-AI/lightning>
- [36] Akiba, T., Sano, S., Yanase, T., Ohta, T., Koyama, M.: Optuna: A Next-generation Hyperparameter Optimization Framework. In: *Proceedings of the 25th ACM SIGKDD International Conference on Knowledge Discovery And Data*

Mining (2019)

- [37] Mesarcik, M., Boonstra, A.-J., Nieuwpoort, R., Rangelova: Learning to detect RFI in radio astronomy without seeing it (2022) <https://doi.org/10.5281/zenodo.6724065>
- [38] Pritchard, N.: pritchardn/SNN-RFI-SUPER. Zenodo (2024). <https://doi.org/10.5281/zenodo.13969016> . <https://zenodo.org/records/13969016>

Acknowledgments

This work was supported by a Westpac Future Leaders Scholarship, an Australian Government Research Training Program Fees Offset and Stipend, and resources provided by the Pawsey Supercomputing Research Centre with funding from the Australian Government and the Government of Western Australia.

Author contributions

N.J.P., A.W., M.B., and R.D. all contributed conceptually. N.J.P. and A.W. conceived the idea. N.J.P. designed and performed the simulations. N.J.P., A.W., M.B., and R.D. wrote the manuscript.

Competing interests

The authors declare no competing interests.

Additional Information

Correspondence

and requests for materials should be addressed to Nicholas J. Pritchard.